PCCP

Accepted Manuscript

ROYAL SOCIETY OF CHEMISTRY

www.rsc.org/pccp

Manipulating the Kinetics and Mechanism of Phase Separation in Dynamically Asymmetric LCST Blends by Nanoparticles

J. Khademzadeh Yeganeh,[a] *F. Goharpey,*[*b] *E. Moghimi,*[c] *G. Petekidis*[c] *and R. Foudazi*[d]

[a] Polymer Engineering Group, Faculty of Engineering, Qom University of Technology, Qom, Iran

[b] Department of Polymer Engineering, Amirkabir University of Technology, Tehran, Iran

[c] IESL-FORTH and Department of Material Science and Technology, University of Crete, GR-711 10 Heraklion, Greece

[d] Department of Chemical and Materials Engineering, New Mexico State University, Las Cruces, NM 88003, USA

ABSTRACT: The addition of nanoparticles in dynamically asymmetric LCST blends is used to induce preferred phase-separating morphology by tuning the dynamic asymmetry, and to control the kinetics of phase separation by slowing down (or even arresting) the domain growth. For this purpose, we used hydrophobic and hydrophilic fumed silica, which self-assemble during phase separation into the bulk of the slow (PS-rich) and fast (PVME-rich) dynamic phase, respectively. Both types of nanoparticles slow down considerably nucleation and growth (NG), spinodal decomposition (SD), and viscoelastic phase separation (VPS) at volume fractions as low as

* Corresponding Author; E-mail: goharpey@aut.ac.ir; Tel: +98 21 64542437.

0.5%. Remarkably, beyond a critical volume fraction of hydrophobic nanosilica thermodynamically controlled phase separation mechanisms (NG and SD) change to VPS mechanism due to enhanced dynamic asymmetry. However, in the presence of hydrophilic nanosilica dynamic asymmetry decreases and beyond a critical particle volume fraction a transition from VPS to SD mechanism is observed. Phase separation is arrested at 2% nanoparticle loading, and VPS percolating networks as well as co-continuous SD structures are completely stabilized by hydrophobic silica or hydrophilic silica, respectively. Electron microscopy images confirm that double percolated structures are induced in the presence of 2 vol% of either hydrophobic or hydrophilic nanoparticles.

1. Introduction

Phase separation of polymer blends still remains a significant scientific challenge that involves complex combinations of kinetics and thermodynamics.[1-4] Controlling the morphological evolution is very important to design various advanced materials with novel mechanical, optical, electrical, and transport properties.[5-10] For example, co-continuous structures in polymer blends form a three-dimensionally percolating network which may synergistically combine the mechanical, electronic, optical, and transport properties of both components.[5-10] As such structures are not thermodynamically in equilibrium, the ability to manipulate them through kinetical trapping is technologically important for applications in photovoltaic cells,[6] resistive switches,[7] and polymer-based membranes.[10]

Thermally-induced phase separation has traditionally been classified into two mechanisms: (i) nucleation and growth (NG), where droplets of the minor phase nucleate and grow spherically with time, and (ii) spinodal decomposition (SD), where highly interconnected structures form in the early stage of phase separation which break up into a droplet-matrix morphology under interfacial tension in later stages.[11] Furthermore, Tanaka found a new and quite unusual phase separation in dynamically asymmetric mixtures, called viscoelastic phase separation (VPS).[12-13] Dynamic asymmetry which comes from the unequal mobility between component molecules can be induced by a large difference in glass transition temperature (T_g) or a large size difference.[12-13] Most of the real mixtures in nature are dynamically asymmetric.[14] Self-generated stresses in the more elastic phase built up during VPS, leading to the induction of a percolating network of the more elastic phase even if it is the minor phase. The network structure coarsens by a volume shrinking process during phase separation and ultimately breaks into disconnected domains where the initially matrix phase becomes the disperse phase at later stages of phase separation

(phase inversion).[12-13,15] In our previous studies on polystyrene/poly(vinyl methyl ether) (PS/PVME) blends,[3] three additional phase separation mechanisms were observed in addition to thermodynamically controlled phase separation mechanisms (NG and SD), due to the self-generated stresses: (i) transient gel induced VPS (TG-VPS), (ii) coalescence induced VPS (C-VPS), and (iii) aggregation induced NG (ANG).

VPS can produce a percolated network structure of the minor phase. Therefore, it is quite useful for designing a heterogeneous structure with advanced mechanical, electrical, and/or biological functions.[1,2,16] However, this structure is of intrinsically nonequilibrium nature and will relax to disconnected domains if it is annealed. Therefore, stabilizing the network structure could open new applications for phase-separating polymer blends. Recently, such stabilization of the non-equilibrium structure in polymer blends through the self-assembly of concentrated colloidal particles at the interface has attracted significant attention.[17-20] There are two groups of colloidal particles that are expected to be strongly adsorbed at the interface leading to pronounced slowing down of the phase separation kinetics:

i. Neutrally wetting particles with equal affinity to both components:[17,18] The stabilization of emulsions by addition of such particles has revealed interesting bicontinuous interfacially jammed emulsion gels (bijels) which are metastable states with interpenetrating, continuous domains of two immiscible fluids.[17,18]

ii. Particles with dual nature (Janus particles), which have different chemistry or polarity on their two hemispheres;[19,20] for example, one side of the particle is hydrophilic, while the other side is hydrophobic.

Therefore, in both cases an efficient stabilization requires careful tuning of the colloidal surface chemistry.[17-20]

Another area, which has come under intense study in polymer blends, is the potential compatibilization of nanoparticles with a preferential affinity to one of components, rather than the interface of phases.[21-25] Such nanoparticles are often commercially available in various sizes with a wide variety of surface treatments in many industrial applications as reinforcing fillers and additives for the control of rheological properties.[26] Experimental studies of phase-separating polymer blends containing selectively wetted and well-dispersed particles show the slowdown of kinetics.[21-24] Li et al.[25] have shown the potential of nanoparticles to kinetically arrest co-continuous morphology in phase-separating polymer blends at a low particle volume fraction due to gelation of the nanoparticles within one of the polymer phases. Moreover, inclusion of nanoparticles does not only induce changes in the kinetics of phase separation, but also modifies the shape of phase diagram.[22,23] While, there are several studies on phase behavior of polymer blends in the presence of nanoparticles, the effect of nanoparticles on the kinetics of phase separation and phase-separating morphology are not well understood. Most of the studies deal with the effect of nanoparticles on the phase diagram, or simply, the influence of nanoparticles on the miscibility of polymer blends.[22,23,27,28] The conditions in which particles slow down or arrest the process of phase separation and the mechanism behind such phenomenon still needs further fundamental studies. It should be noted that the introduction of particles to polymer blends significantly increases the system complexity due to the additional particle-particle and particle-polymer interactions, and modifies their rheological properties.

In our previous work,[29] we have demonstrated that the kinetics of viscoelastic phase separation can be efficiently suppressed through the addition of hydrophobic nanoparticles that are selectively incorporated in the PS-rich phase during the phase separation. Moreover, beyond a critical nanoparticle volume fraction, phase separation is pinned due to particle percolation

within the PS-rich phase, yielding a kinetically trapped VPS-induced network structure. Other studies in the literature on the control of phase separation kinetics focus mainly in the case of normal phase separation mechanisms.[23,25,28] Laradji and McNevin[30] and Zhu and Ma[31] studied through computer simulations the effect of nanoparticles with a preferential affinity to one of components on the compatibility of polymer blends and phase separation kinetics. These studies showed that the phase separation is slowed down in the presence of nanoparticles. Balazs and co-workers investigated phase separation of a binary polymer blend containing nanoparticles using both kinetic theories and computer simulations.[32-34] They found that in the case of preferential affinity to one of polymer components, particles slow down the growth of domains in the late stage of spinodal decomposition. However, simulations of the effect of nanoparticles on the phase separation kinetics have been restricted to "dynamically symmetric" mixtures.[30-34] In view of the above and our previous experimental findings,[29] we believe that the addition of nanoparticles with preferential affinity to one of the components in dynamically asymmetric mixtures opens up wider possibilities for efficient tuning of such systems while fundamental questions on the underlying mechanisms are still open.

In this work, we use PS/PVME model phase-separating system, which exhibits a lower critical solution temperature (LCST) within the experimental temperature window.[35] Both polymers are fully amorphous and the large difference in their glass transition temperatures (about 125 ^{o}C) makes their blends dynamically asymmetric. The main objective of this work is to investigate the addition of nanoparticles with a preferential affinity to one of the components as a potential route to induce desired phase-separating morphologies by tuning the dynamic asymmetry, as well as to control the kinetics of phase separation by slowing down or arresting the domain growth. For this purpose, two different types of fumed silica nanoparticles were used: hydrophobic nanoparticles

that preferentially wet the slow dynamic phase (PS-rich phase), and hydrophilic ones that preferentially wet the fast dynamic phase (PVME-rich phase).

2. Experimental Section

2.1. Materials. A commercial grade PS (polystyrene) supplied by Tabriz Petrochemical Co. (GPPS grade 1460), and PVME (polyvinyl methyl ether), Lutonal M40, supplied by BASF Co., were used. The basic characteristics of the polymers are listed in Table 1. Two different commercial fumed silica nanoparticles (Degussa Corporation) with average particle size of 12 nm, density of 2.2 g/cm^3 and specific surface area equal to 200 m^2/g were used: Aerosil 200 with hydrophilic surface due to the free silanol groups and Aerosil R974 with hydrophobic surface due to the modification with dimethyldichlorosilane.

Table 1. Characterization of PS and PVME used in this study.

	M_w (g/mol)	M_n (g/mol)	T_g (^{o}C)	Supplier
PS	340000	130000	95	Tabriz Petrochemical Co.
PVME	110000	64000	-28.6	BASF

2.2. Sample Preparation. The neat PS/PVME blends are denoted by M/N and PS/PVME/nano blends are denoted by M/N/x; where M and N stand for weight fractions of PS and PVME in the blend, respectively; while x denotes the volume fraction of the nanoparticles as compared to the total amount of polymers. The blends of PS/PVME in the two-phase region were prepared by continuous mechanical mixing of the components in toluene for 24 hours.[23,36] The compositions of PS-rich and PVME-rich phases were obtained from tie-lines in the phase diagram at selected temperatures.[36,37] Such samples, which are in the miscible region, were prepared similarly to

other PS/PVME blends. To prepare samples containing nanoparticles, the required amount of nanoparticles was dispersed in toluene after probe ultrasonication for 30 min, and the dispersion was then mixed with the PS/PVME solution and stirred for 24 hr. Silica nanoparticles were dried at 100 ^{o}C for 24 h prior to use.

A 0.05 wt % Irganox 1010 (Ciba-Geigy Group) was added to the mixtures to prevent the thermal oxidation during preparation and measurements. It should be noted that the added antioxidant does not change the glass transition temperature of the blend nor the temperature of the thermally induced phase separation.[38] The solvent was evaporated slowly at room temperature for 1 week. Then, the samples were put in a vacuum oven for 4 days at 45 °C. The vacuum was applied slowly to prevent any possible bubble formation. Finally, the full vacuum was applied at 70 °C for 24 hr in order to remove the residual solvent remaining in the samples. Samples for optical microscopy were prepared similarly. However, the thickness of samples for optical microscopy (OM) was approximately 25-30 μm . This is considerably thicker than the critical thickness (5-8 μm thin films) found by Reich and Cohen[39] above which there is no dependence of the phase behavior on the film thickness and substrate.

2.3. Methods.

Rheological Measurements: Rheological tests were carried out using an Anton Paar MCR-501 rheometer with parallel plate geometry of 25 mm diameter and a sample gap of 1 mm. Temperature control of ±0.1 °C was achieved with a Peltier system under a nitrogen atmosphere. All experiments were carried out in the linear regime (1% oscillatory strain amplitude), as was verified by preliminary dynamic strain amplitude sweep tests. Isochronal dynamic temperature sweep tests were carried out to detect the onset of phase separation by measuring storage and loss moduli, G' and G'', at a fixed frequency of ω=0.3 rad/s (low enough to be in the terminal

flow regime according to literature data[23,36]) and a uniform heating rate of 0.5 °C/min.[23,40] Dynamic time sweep experiments for 16 hr were performed in the two-phase region at a fixed frequency of 1 rad/s to investigate the phase separation kinetics. According to Kim et al.[41] rheological measurements under such conditions can sensitively detect the early stage of phase separation. Finally, dynamic frequency sweep experiments were carried out to study the linear viscoelastic properties of phase-separated domains.

Optical Microscopy (OM): The phase contrast optical microscopy (Leica DMRX) was used to investigate the morphological changes at different quench depths. Samples were placed in a hot stage sample holder (Linkam LTS350) controlled by Linkam CI 94 controller. Fresh nitrogen gas was circulated in the heating chamber of OM to avoid any possible thermal degradation. A CCD camera mounted directly on the microscope was used to record the evolution of blends structure in real time.

Transmission Electron Microscopy (TEM): Transmission electron microscopy (TEM) images of the samples were obtained with a JEOL JEM-2100 high-resolution transmission electron microscope (HR-TEM) operating at 100 keV. The PS-rich phase of unstained samples is visually darker in TEM micrographs. PVME is more electronegative (due to its ether bond) and absorbs electrons stronger than PS, thus it appear brighter.[25,42]

Differential Scanning Calorimetry (DSC): DSC (Perkin-Elmer, Pyris 1) measurements were carried out under a nitrogen gas atmosphere at a rate of 10 ^{o}C min^{-1} to determine the T_g and ΔC_p of the phase-separated PS-rich and PVME-rich domains. T_g was determined as the temperature corresponding to half the complete change in heat capacity.

Tensile tests: Uniaxial tensile tests were carried out using dumbbell samples in a universal testing machine (Galdabini Sun 2500) with a constant loading speed of 100 mm/min at room temperature.

3. Results and Discussions

3.1. Phase diagram

To obtain the phase diagram of PS/PVME blend with and without nanoparticles, isochronal dynamic temperature sweep experiments were carried out. A typical curve of variation of the storage modulus, G', with temperature is shown in the inset of Figure 1 for the PS/PVME 60/40 blend without and with 2% (by volume) R974 and A200 nanoparticles. For all samples in the homogeneous regime, the elastic modulus decreases with increasing temperature at low temperatures. As the temperature approaches the phase separation temperature, the thermodynamic forces and induction of interfacial energy lead to an increase of G'. The temperature where G' exhibits a minimum is assigned as the phase separation temperature.[43] Obtaining the phase separation temperature of PS/PVME blend by rheological measurements has been explained comprehensively in our previous works and the references therein.[23,44] Figure 1 shows the rheologically obtained phase diagrams of neat PS/PVME blends and the ones filled with 2 % R974 and A200 nanoparticles. The phase diagrams exhibit lower critical solution temperature (LCST) behavior with the critical points located at weight composition of about 20% PS. The phase separation temperatures of the filled PS/PVME blends shift upward by 2–7 ^{o}C with respect to the neat blend.

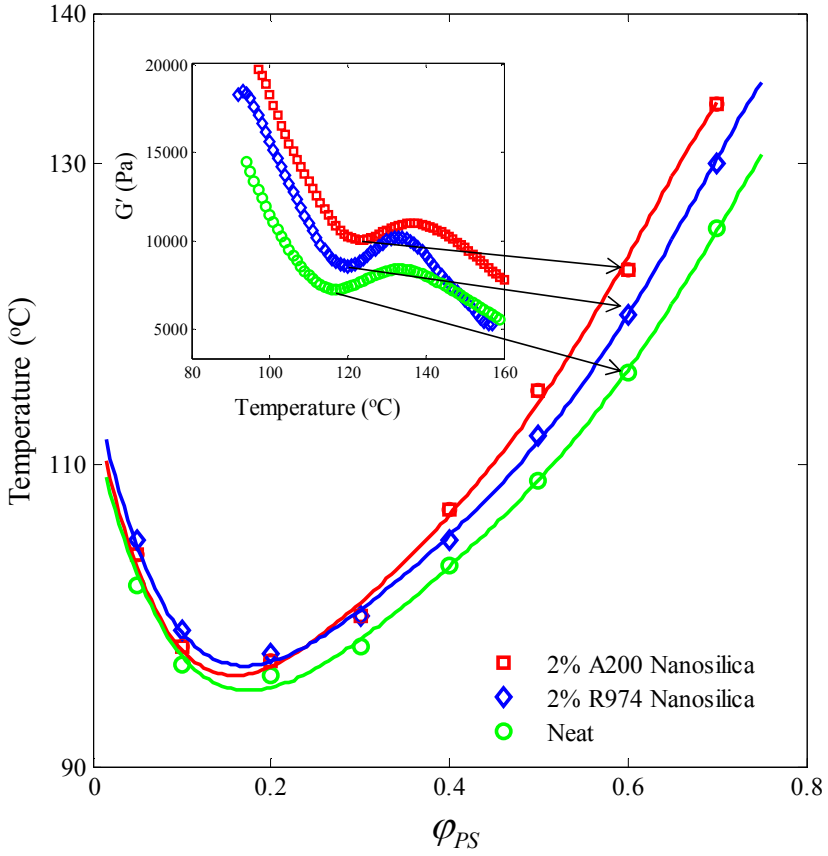

Figure 1. Phase diagram of the neat PS/PVME and PS/PVME/nano blends obtained from rheological measurements (solid lines are guides to the eye). The inset shows the temperature dependence of storage modulus, *G'*, for the neat PS/PVME 60/40 and corresponding blends filled with 2 % R974 and A200 nanoparticles.

The increase in phase separation temperature significantly depends on the blend composition. Figure 1 indicates that nanosilica can enhance the miscibility of PS/PVME blends more efficiently for compositions far from the critical point. Gao et al.[22] and Huang et al.[27] also observed the same behavior in the case of PMMA/SAN blend in presence of SiO_2 nanoparticles. The phase diagrams of the filled PS/PVME blends with 0.5 and 1% R974 and A200 nanoparticles (not shown here) shifted upward by 1–2 ^{o}C and 1–4 ^{o}C, respectively.

The quantitative analysis is possible through the theoretical approach of Ajii and Choplin[45] for homopolymer blends. This is an extension of Fredrickson and Larson's theory[46] for block copolymer melts near the order–disorder transition, providing an expression for G' and G'' in terminal one-phase region in the vicinity of critical point:

$$G'(\omega) = \frac{k_B T\,\omega^2}{240\pi}\left[\frac{1}{3}\left\{\frac{R_{g1}^2}{\phi_1 N_1} + \frac{R_{g2}^2}{\phi_2 N_2}\right\}\right]^{1/2}\left[\frac{1}{\phi_1 b_1^2 W_1} + \frac{1}{\phi_2 b_2^2 W_2}\right]^2 \left[2(\chi_s - \chi)\right]^{-5/2} \quad (1)$$

$$G''(\omega) = \frac{k_B T\,\omega}{240\pi}\left[\frac{1}{3}\left\{\frac{R_{g1}^2}{\phi_1 N_1} + \frac{R_{g2}^2}{\phi_2 N_2}\right\}\right]^{1/2}\left[\frac{1}{\phi_1 b_1^2 W_1} + \frac{1}{\phi_2 b_2^2 W_2}\right]^2 \left[2(\chi_s - \chi)\right]^{-1/2} \quad (2)$$

where ω is the angular frequency, k_B is the Boltzmann coefficient, χ is the interaction parameter at temperature T, χ_s is its value at the spinodal temperature, N_i is the number of statistical segments of species i, with segment length b_i, radius of gyration R_{gi}, volume fraction ϕ_i , and rate of its reorientation W_i. Using the above equations, the following ratio can be defined:

$$\frac{G'(\omega)}{\left[G''(\omega)\right]^2} = \frac{30\pi}{k_B T}\left\{\frac{b_1^2}{36\phi_1} + \frac{b_2^2}{36\phi_2}\right\}^{3/2}(\chi_s - \chi)^{-3/2} \quad (3)$$

Furthermore, the correlation length, ξ , for polymer blends near the critical region can be obtained by random phase approximation (RPA) as follows:[45]

$$\xi = \frac{a'}{6}\left[\phi(1-\phi)(\chi_s - \chi)\right]^{-1/2} \quad (4)$$

where a' is a characteristic length, related to the individual segment lengths, a_1 and a_2 , as follows:

$$\frac{a'^2}{\phi(1-\phi)} = \frac{a_1^2}{\phi} + \frac{a_2^2}{(1-\phi)} \quad (5)$$

Therefore:

$$\xi = \left[\frac{k_B T}{30\pi}\frac{G'}{G''^2}\right]^{1/3}\frac{1}{\phi(1-\phi)} \qquad (6)$$

Hence, the correlation length can be measured near the critical point directly from shear rheological data obtained from the isochronal temperature sweep experiments. The correlation length in general reflects the length scale of concentration fluctuations.[47] Its determination from the rheology using Equation 6 has been proven to agree reasonably well with the estimation from small angle neutron scattering.[45] Figure 2 shows the variations of correlation length with temperature in the vicinity of phase separation temperature calculated from Equation 6 for the neat PS/PVME 20/80 critical blend and neat 60/40 off-critical blend and blends filled with 2% R974 and A200 nanoparticles.

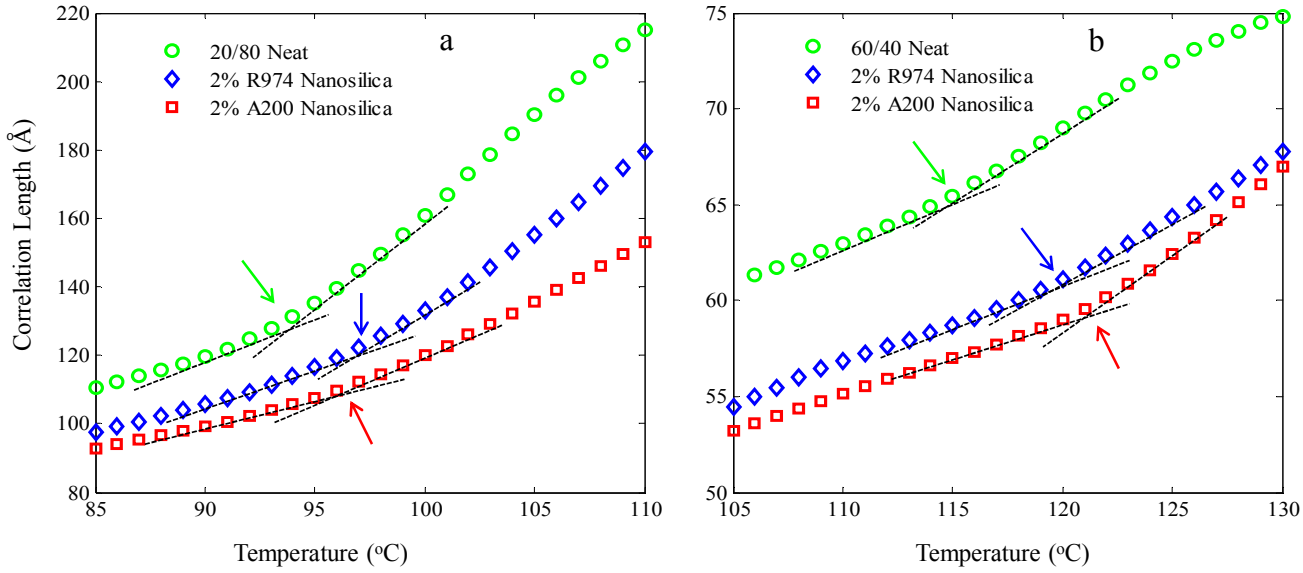

Figure 2. Temperature dependence of the correlation length obtained quantitatively from the isochronal dynamic temperature sweep data for the PS/PVME blends without and with 2% R974 and A200: (a) 20/80 (b) 60/40. Dashed lines are guides to the eye.

In the vicinity of phase separation temperature (indicated with arrow in Figure 2), the increase in correlation length becomes more intense reflecting enhanced local concentration fluctuations by phase separation. The magnitude of the correlation length and its rate of increase with temperature rise are considerably higher for blends with 20% PS than the ones with 60% PS. This means that the kinetics of phase separation for 20/80 blend is faster than the 60/40 one since at the critical composition spinodal concentration fluctuations are expected to be much stronger than at an off-critical composition.

It should be noted that while the effect of nanoparticles on the phase separation temperature is only about 2 ^{o}C for the 20/80 blend, they considerably decrease the correlation length (by about 18-60 Å depending on temperature) with respect to the neat blend. Note that the decrease in correlation length is only about 7-10 Å in the case of the 60/40 blend in presence of nanoparticles. These results suggest that at the critical composition the nanoparticles predominantly change the kinetics rather than thermodynamics of phase separation.

3.2. Morphological observations

3.2.1. Localization of the nanoparticles

Upon increasing the temperature into the two-phase region, the system reduces the free energy through inclusion of particles into the favorable phase (PS-rich, PVME-rich or at the interface) and coarsening of the phase-separated domains (decreasing interfacial area).

In binary mixtures the affinity of nanoparticles to any of the components, and thus the localization of nanoparticles in the two-phase region, can be predicted by the wetting coefficient ω_{12}:[48]

$$\omega_{12} = \frac{\Gamma_{s-PVME} - \Gamma_{s-PS}}{\Gamma_{12}} \qquad (7)$$

where Γ_{12} is the interfacial tension between PS and PVME, and $\Gamma_{s-Polymer}$ is the interfacial tension between the particle and polymer. When $\omega_{12} > 1$, the affinity of particles to the PS is more than to the PVME; thus, it is expected that nanoparticles will be incorporated preferentially in the PS-rich phase during the phase separation. Similarly, for $\omega_{12} < -1$, nanoparticles will be expected to penetrate in the PVME-rich phase, and if $-1 < \omega_{12} < 1$, they will be localized at the interface of phase-separated domains.

Estimation of the interfacial tension between two components 1 and 2 is achieved using the well-known Owens and Wendt equation:[48,49]

$$\Gamma_{12} = \Gamma_1 + \Gamma_2 - 2\sqrt{\Gamma_1^d \Gamma_2^d} - 2\sqrt{\Gamma_1^p \Gamma_2^p} \quad (8)$$

where the superscripts *d* and *p* stand for the dispersive and the polar contributions to the surface tension, respectively. Surface tension data of the components of the blends are given in Table 2. According to Equation (7) the wetting coefficients for our polymer systems containing R974 and A200 nanoparticles are 2.88 and -2.53 respectively. Therefore, as will be confirmed by TEM micrographs, R974 particles are expected to be strongly driven by the thermodynamic forces into the bulk of PS-rich phase, while A200 particles should concentrate in PVME-rich phase to reduce the free energy of the system during the phase separation.

Table 2. Surface tension data of the components of the blends.

	$\Gamma(mN/m)$	Γ^d	Γ^p
PS[1]	40.7	34.5	6.1
PVME[2]	59.5	35.5	24
A200 silica[3]	80	29.4	50.6
R974 silica[4]	18	18	0

[1,3] From reference 50.

[2,4] From reference 29.

3.2.2 Neat PS/PVME and PS/PVME/R974 blends

We carried out optical microscopy observations for PS/PVME blends with weight compositions of 15/85, 30/70 and 40/60, which phase separate, in the absence of nanosilica at constant temperature of 110 ^{o}C, through TG-VPS, SD, and NG, respectively. These samples contained 0, 0.5, 1, and 2 vol% of R974 or A200. The inset of each optical micrograph corresponds to two-dimensional fast Fourier transform pattern, 2D-FFT, obtained by ImageJ software. For systems undergoing spinodal decomposition, the 2D-FFT pattern develops a distinct scattering ring (spinodal ring).[51,52] However, for samples phase separating by NG no scattering ring is observed.[51,52] There is no study on FFT pattern in the VPS region. At first we discuss the effects of R974 hydrophobic nanosilica on the phase separation mechanisms and morphological evolution of phase-separating PS/PVME blends, and then, we present the results of samples filled with A200 hydrophilic silica.

Viscoelastic phase separation region, PS/PVME 15/85 blend.

As shown in Figure 3a, the neat PS/PVME 15/85 blend undergoes viscoelastic phase separation at 110 ^{o}C. Major PVME-rich phase nucleates and grows in the minor PS-rich matrix phase, accompanied by volume shrinkage of the matrix that leads to the formation of a PS-rich network structure. In the late stage, a morphological transition from network structure to disperse-matrix morphology occurs. The surface fraction of the PS-rich phase decreases from 80% in the early stages of phase separation to 25% in the late stage due to volume shrinking. In VPS, self-induced stresses in the component with higher T_g mainly cancel the stress originated from the surface tension, leading to its continuity even if it is a minority phase.[13,15] It can be seen that for samples undergoing VPS no ring formation is observed in the corresponding 2D-FFT patterns similar to NG mechanism. In fact VPS mechanism can be considered as nucleation of major phase (PVME-rich) in the minor phase (PS-rich) resulting in the observed pattern.

Figure 3b shows the morphology development of PS/PVME 15/85 blend containing 0.5% R974 nanosilica at 110 ^{o}C, in which the phase separation proceeds by TG-VPS similar to the neat blend. However, the growth of PVME-rich domains, or kinetics of phase separation, decreases with the addition of nanosilica. Similar trend is observed for sample containing 1% R974 nanosilica (not shown here). The slower kinetics of phase separation in the presence of nanoparticles can be attributed to the diffusion of frustrated PS chains with preferential affinity to the surface of hydrophobic nanosilica. Therefore, an adsorbed layer of PS segments with decreased mobility forms at the surface of hydrophobic nanoparticle.[53,54]

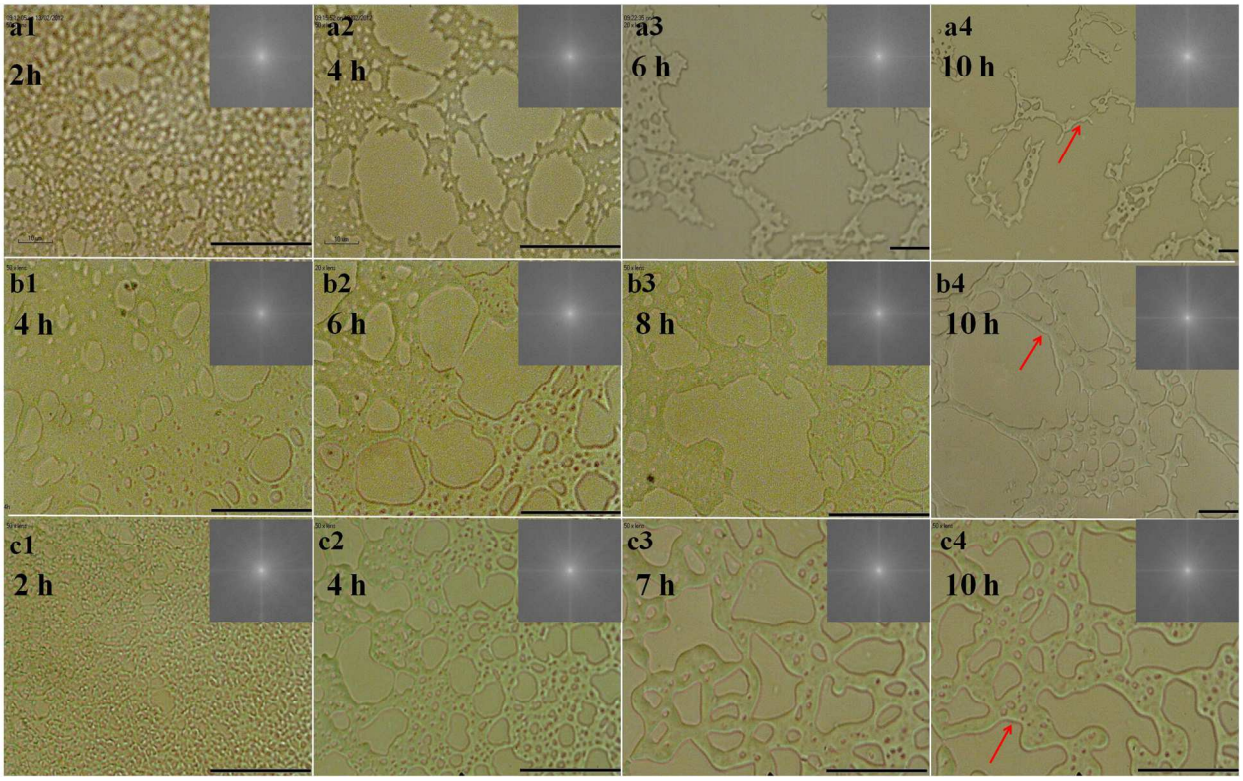

Figure 3. Optical micrographs indicating time evolution of the phase-separating morphologies at 110 ^{o}C for PS/PVME 15/85 blend containing R974 nanosilica with volume fraction of: (a) 0%, (b) 0.5%, and (c) 2%. All the scale bars correspond to 30 μm . The insets show correspondding two-dimensional fast Fourier transform pattern, 2D-FFT. The red arrows indicate PS-rich phase.

Figure 3b shows that PS-rich network does not rupture in the sample containing 0.5% nanosilica even after a long period, which can be related to the enhanced dynamic asymmetry and also improvement of the mechanical properties of PS-rich phase in the presence of nanoparticles. The nanoparticles will be selectively localized in the PS-rich phase, thus enhancing the dynamic asymmetry between the PS-rich and PVME-rich phases (as will be shown by DSC and rheological measurement). As dynamic asymmetry increases, self-generated stresses are strengthened, and thus, inhibit the disintegration of network structure. Our experimental

observations are consistent with the simulation work reported by Zhang et al.[15] on VPS of binary mixtures, in which the dynamic asymmetry could be changed in the constitutive equations of simulation. Their results show that the phase inversion is prolonged and the network structure persists for a longer period by increasing dynamic asymmetry.

During VPS, the network is stretched continuously and elongated under self-generated stresses that are concentrated selectively on the thinnest (weakest) stretched parts.[55,56] Therefore, the mechanical properties of PS-rich phase which forms the network structure can be a controlling factor in VPS kinetics. Figure 4 shows the stress−strain behavior of the PS-rich phase in the presence of various contents of R974 nanoparticles. According to the phase diagram, the composition of the PS-rich phase is about PS/PVME 50/50 at 110 ^{o}C (determined by the tie line in the phase diagram), which can be prepared as explained in the Experimental Section. According to the lever rule,[44] the volume fraction of phase-separated PS-rich phase is about 25% for the studied PS/PVME samples at 110 ^{o}C. Therefore, the local volume fraction of nanoparticles in PS-rich phase will be about 2% and 4% for PS/PVME 15/85 blends filled with 0.5% and 1% nanosilica, respectively.

The Young's modulus, strain-at-break, and the area under the stress-strain curve which is a measure of the ability of a material to absorb energy up to fracture, increase monotonically by increasing the nanoparticle loading. In agreement with literature, the addition of nanofiller can significantly enhance the mechanical properties of polymeric materials.[57,58] Thus, a higher energy or stretching force is required to rupture the PS-rich phase containing nanoparticle than the neat one, which leads to a longer-lived PS-rich network structure.

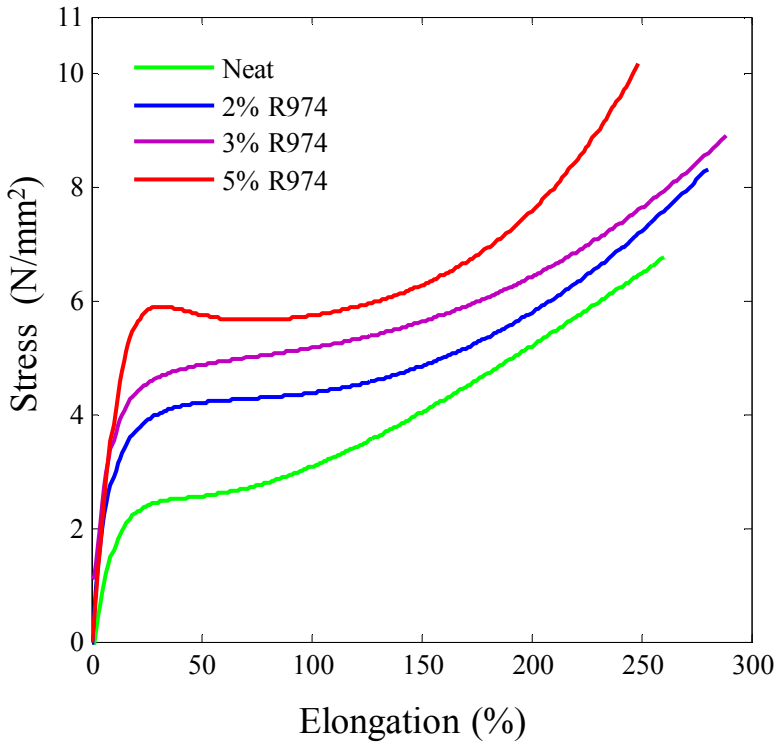

Figure 4. The stress–strain behavior of PS-rich phase containing different amounts of R974 nanosilica at room temperature.

Figure 3c shows that the phase separation of PS/PVME 15/85 blend containing 2% R974 nanosilica at 110 ^{o}C also undergoes VPS mechanism. Remarkably, the percolated PS-rich network structure becomes extremely stable after about 5 hr from the onset of phase separation. In other words, only 2 % hydrophobic nanosilica can kinetically pin (arrest) network structure induced by VPS in PS/PVME blend.

Figure 5 shows the TEM images of PS/PVME 15/85 sample containing 2% nanosilica before phase separation and after 7 hr annealing at 110 ^{o}C. The dark spots in Figure 5a depict the nanosilica particles since PS and PVME are still in the one-phase state. In Figure 5b, the darker region is the PS-rich phase (as described in the Experimental section), which has now engulfed the nanosilica particles as well. The TEM micrographs indicate that small clusters of

nanoparticles are properly distributed in the miscible blend before annealing. However, after 7 hours of annealing in the two-phase region, aggregates of nanoparticles have diffused entirely into PS-rich phase, away from the interface, in agreement with the prediction of Equation 7.

The strong unfavorable enthalpic interaction between hydrophobic R974 nanoparticles and polar PVME chains induces self-assembly of nanoparticles into the PS-rich phase. Consequently, the system forms a double percolating structure: the network of nanoparticles is induced in the network of PS-rich phase. Double percolation refers to the percolation of a filler within one phase of a polymer blend (first percolation), which itself percolates in the blend (second percolation).[59-61]

The mechanism of pinning can be explained as follows. When the sample is quenched into the two-phase region, the system spontaneously separates into distinct PS-rich and PVME-rich phases. Thus, particles are pushed by thermodynamic forces into the energetically favorable PS-rich phase and aggregate into clusters of increasing size. As the phase separation proceeds, the nanoparticle concentration increases in the shrinking PS-rich phase and subsequently a percolated network of nanoparticles is formed. So, as observed in the TEM micrograph, hydrophobic nanosilica particles are localized selectively in the PS-rich phase of phase-separated blends. The local volume fraction of nanoparticles in PS-rich phase will be about 8% for sample filled with 2% nanosilica. Since the concentration of nanoparticles is much higher than the percolation threshold of nanosilica,[62] the aggregation and percolation are promoted in the two-phase region of the filled polymer blends studied here. When nanoparticles form a relatively stable structure within the PS-rich phase with a characteristic size comparable to the characteristic domain size of PS-rich network, the domain growth is pinned. In addition, the

phase containing nanoparticles becomes solid-like, and consequently, the hydrodynamic flow is suppressed, and the shape relaxation of the domains by interfacial tension becomes inefficient.

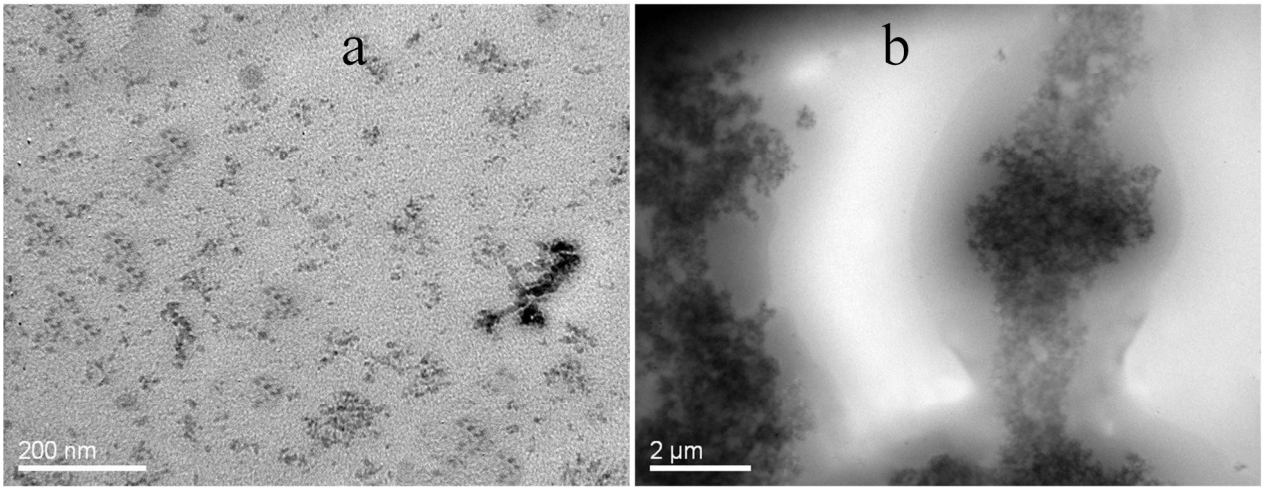

Figure 5. TEM micrographs of PS/PVME/R974 15/85/2 blend: (a) before annealing, and (b) after 7 hr annealing at 110 ^{o}C.

Spinodal decomposition region, PS/PVME 30/70 blend.

Figure 6a shows PS/PVME 30/70 blend undergoes spinodal decomposition at 110 ^{o}C yielding a highly interconnected structure in the early stages of phase separation. The corresponding scattering ring from the 2D-FFT suggests that the phase separation process occurs through spinodal decomposition. A considerable free energy is stored at highly curved interface between the phases in a co-continuous morphology. Thus, thermodynamic equilibrium favors breakup of co-continuous structure into droplet-matrix morphology. At later stages, droplets grow dramatically with a broad size distribution.

In the presence of 0.5% R974 nanosilica (not shown here), SD mechanism still controls the phase separation, but with a slower kinetics. Upon increasing the volume fraction of

nanoparticles further to 1%, SD mechanism disappears and TG-VPS controls the phase behavior (Figure 6b); since nonspherical droplets of PVME-rich forms in the PS-rich in the early stages of phase separation and grow by time. At later stages, PS-rich phase transforms into a sponge-like structure. However, the formed network by TG-VPS in this sample shows phase inversion after a long times (12 hr). The transition of phase separation mechanism from SD to VPS can be ascribed to the enhancement of dynamic asymmetry between the phase-separating domains in the presence of hydrophobic nanoparticles. The increase in dynamic asymmetry strengthens the stress fields; consequently, the elastic energy dominates the phase separation and the system behaves like an elastic gel in the initial stage of phase separation. To the best of our knowledge, this is the first time that transition of SD to VPS by tuning the dynamic asymmetry is reported.

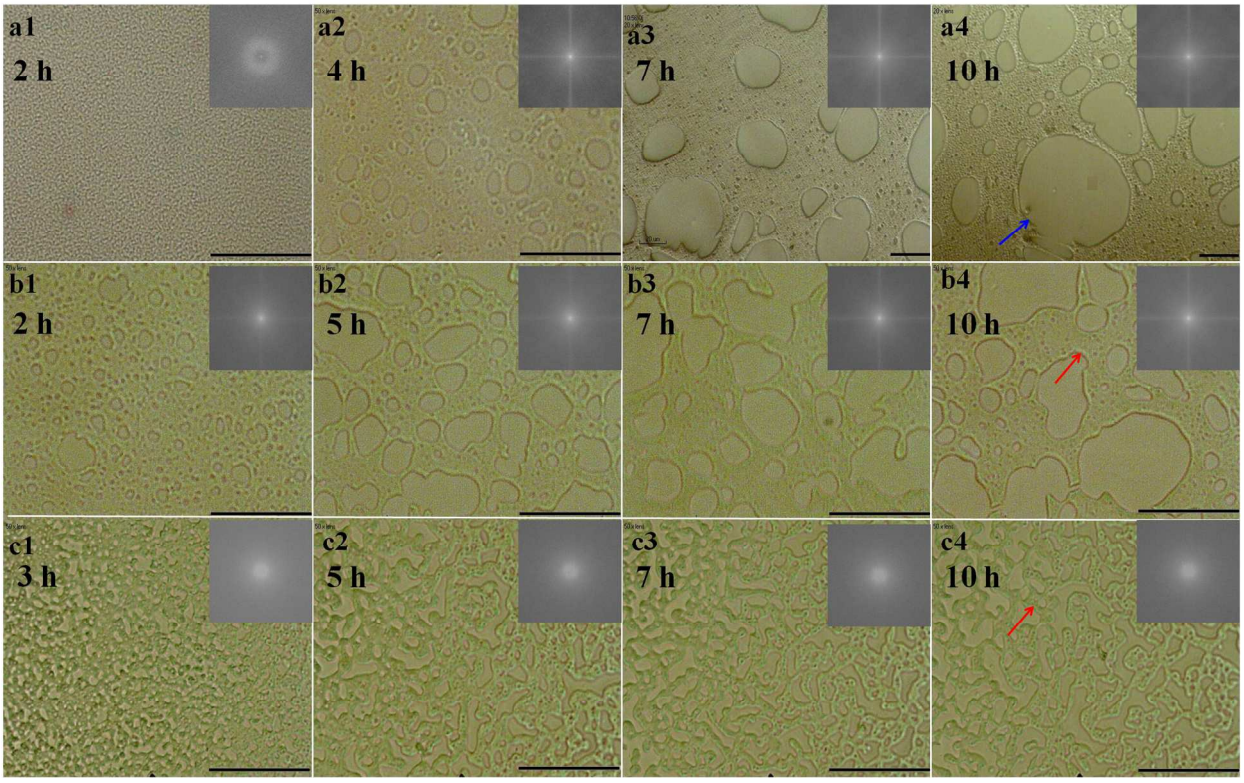

Figure 6. Optical micrographs indicating time evolution of the phase-separating morphologies at 110 ^{o}C for PS/PVME 30/70 blend containing R974 nanosilica with volume fraction of: (a) 0%, (b) 1%, and (c) 2%. All the scale bars correspond to 30 μm . The insets show correspondding two-dimensional fast Fourier transform pattern, 2D-FFT. The red and blue arrows indicate PS-rich and PVME-rich phases, respectively.

The early stages of SD and VPS have similar driving forces since the thermodynamic osmotic force, Π, causes the diffusional motion of molecules and the usual growth of concentration fluctuations. In the dynamically asymmetric mixtures, however, this motion induces the stresses, σ, in the component with the higher relaxation time. According to the dynamic equations developed by Tanaka[63] to describe the viscoelastic phase separation, these are the two opposing forces that determine the evolution of the systems according to Π–σ. For a sample in the SD

region, strong concentration fluctuations cancel the self-generated stresses and phase separation proceeds in the usual way. However, for a sample in VPS region the initial growth of concentration fluctuations is significantly suppressed and the phase separation becomes frozen. For the 30/70 blend, beyond the critical volume fraction of nanosilica, 1%, the enhanced dynamic asymmetry overcomes the thermodynamic forces, and VPS controls the phase behavior. With further increasing the amount of nanoparticles to 2% in the PS/PVME 30/70 blend, VPS overcomes SD and controls the phase behavior similar to the sample containing 1% nanosilica (Figure 6c). However, the sample containing 2% R974 has a finer PS-rich network and after about 5 hr of annealing, the percolated PS-rich network remains unchanged suggesting the structure is pinned. The pinning mechanism is similar to the one suggested for the PS/PVME/R974 15/85/2 blend.

We further study the origin of the enhanced dynamic asymmetry in the presence of nanosilica utilizing DSC and rheological measurements. As the phase separation proceeds, thermodynamic forces push nanoparticles into the energetically favorable PS-rich phase, which has PS/PVME 50/50 composition at 110 ^{o}C as mentioned before. As seen in Figure 7a, the T_g of the PS-rich phase increases significantly with the addition of hydrophobic nanosilica. Therefore, there is an attractive interaction between polymer molecules and nanoparticles, which restricts the chain mobility in the PS-rich phase, and thus, enhances the dynamic asymmetry between PS-rich and PVME-rich phases.

The value of the heat capacity is proportional to the number of internal molecular degrees of freedom (chain mobility). Therefore, the change of heat capacity (ΔC_p) at glass transition temperature by addition of nanosilica can be an estimate of the change in polymer chain mobility.[64] The values of ΔC_p at glass transition temperature for PS-rich phase with different

concentrations of nanosilica are shown in Figure 7b. As more nanofillers are introduced into the system, more polymer chains will interact with nanoparticles, which will decrease the average degree of freedom for the polymer segments; and thereby, ΔC_p decreases with increasing nanoparticle content.

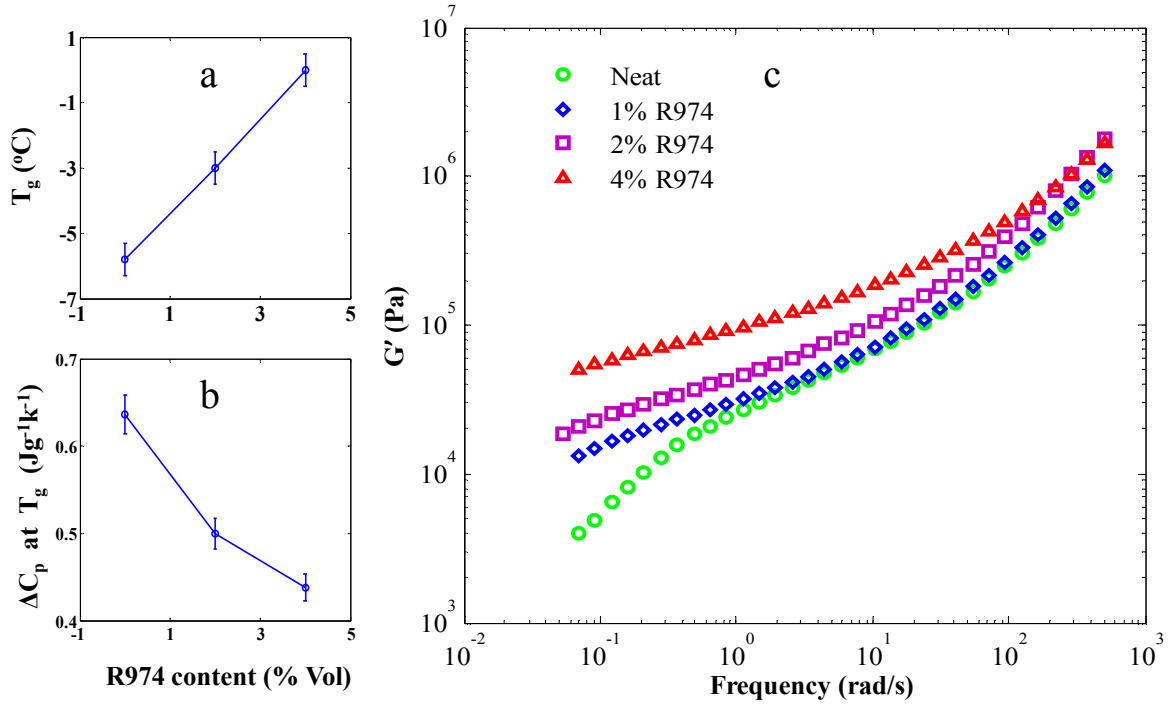

Figure 7. a) Values of T_g for the PS-rich phase as a function of nanosilica content; b) change in heat capacity (ΔC_p) of PS-rich phase at glass transition as a function of nanosilica content; and c) frequency-dependent storage modulus of PS-rich phase containing different volume fractions of R974 nanosilica at 110 °C. Vertical lines in parts a and b represent error bars.

Figure 7c shows the elastic modulus, G', as a function of angular frequency, ω, for PS-rich phase with different concentrations of nanoparticles at 110 °C. As the particle loading increases, the dependence of low frequency G' on ω weakens and the elastic modulus G' increases especially at low frequencies. Thus, the long-range dynamics of chains in the PS-rich phase are restrained in

the presence of hydrophobic nanoparticles, and thus, the dynamic asymmetry between the PS-rich and PVME-rich phases is enhanced. At high frequencies, the effect of nanoparticles on the rheological behavior is relatively weak suggesting that the hydrophobic nanoparticles do not significantly influence the short-range dynamics of polymer chains, particularly in the entanglement length scales.[65]

Nucleation and growth region, PS/PVME 40/60 blend.

Figure 8a shows the morphological evolution of PS/PVME 40/60 blend at 110 ^{o}C. In the early stage of phase separation, PVME-rich droplets nucleate and grow up in size indicating that the NG mechanism controls the phase behavior in this sample.

Upon incorporation of 0.5% nanosilica, phase separation still proceeds by NG mechanism (Figure 8b). However, such a small amount of hydrophobic nanosilica substantially slows down the kinetics of phase separation in which PVME-rich droplets are much smaller at corresponding phase separation times with respect to the neat blend. Similar behavior is observed for sample containing 1% R974 nanosilica (not shown here). It may be suggested that the hydrophobic silica dispersed in miscible PS/PVME blend at room temperature, act as a nucleating agent upon the onset of phase separation.

In general, droplet coarsening in phase-separating mixtures occurs under two different mechanisms: (i) the evaporation-condensation mechanism (EC) or Ostwald ripening,[66] and (ii) the Brownian-coagulation mechanism (BC), where random collision of droplets can result in coalescence.[67] According to the EC mechanism, the bigger droplets grow at the expense of smaller ones by diffusion of material through the continuous phase into the larger droplets. Nanoparticles increase the viscosity of PS-rich matrix and also act as a physical barrier in the

matrix phase. Therefore, the addition of nanoparticles: (i) prevents the movement of the PVME-rich droplets to coalesce (BC mechanism), and (ii) decreases the diffusional motion of PVME-rich molecules through PS-rich matrix (EC mechanism). Consequently, the nanoparticles considerably slow down the kinetics in the NG mechanism.

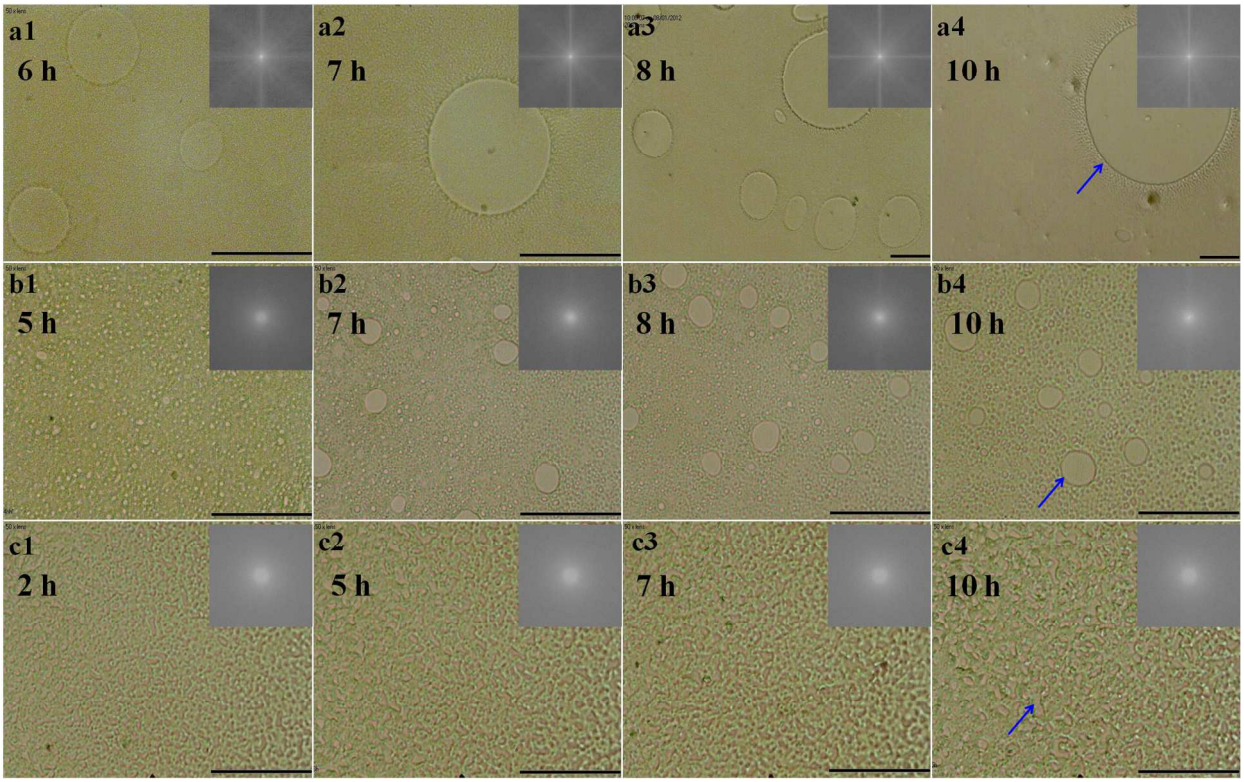

Figure 8. Optical micrographs indicating time evolution of the phase-separating morphologies at 110 ^{o}C for PS/PVME 40/60 blend containing R974 nanosilica with volume fraction of: (a) 0%, (b) 0.5%, and (c) 2%. All the scale bars correspond to 30 μm . The insets show correspondding two-dimensional fast Fourier transform pattern, 2D-FFT. The blue arrows indicate PVME-rich phase.

Figure 8c shows the morphology development of PS/PVME/R974 40/60/2 blend at 110 ^{o}C. As seen NG mechanism disappears in this sample and VPS controls the phase behavior inducing an arrested PS-rich network with a fine structure. To the best of our knowledge, this is the first time that transition of thermodynamically-driven NG to VPS is accomplished through tuning the dynamic asymmetry.

The dynamic asymmetry between PS-rich and PVME-rich phases can be characterized by a dynamic asymmetry parameter ξ which is given as:[12,68]

$$\xi = \frac{\tau_1}{\tau_2} \qquad (9)$$

where τ_1 and τ_1 are the relaxation time of the slow and fast components, respectively (in this work, PS-rich and PVME-rich phases, respectively). To express the relative change of dynamic asymmetry after the addition of nanoparticles, a parameter $\frac{\Delta\xi}{\xi_{neat}}$ is defined as:

$$\frac{\Delta\xi}{\xi_{neat}} = \frac{\xi_{nano} - \xi_{neat}}{\xi_{neat}} \times 100 \qquad (10)$$

where ξ_{neat} and ξ_{nano} are the dynamic asymmetry of neat PS/PVME blends and that of PS/PVME/nano blends, respectively. The relaxation times of the phase-separated domains were obtained by rheological measurements through plotting the weighted relaxation time spectrum, $\tau H(\tau)$, as a function of relaxation time, τ, as described in our previous work.[44] Figure 9 shows relative change of dynamic asymmetry versus the volume fraction of R974 nanosilica for studied PS/PVME blends. It should be noted that to obtain the relaxation times of the phases, the volume fraction of the nanoparticles in each phase is required. For this purpose, we considered that all the R974 nanoparticles are included in the PS-rich phase (as observed by TEM image) and the volume fraction of separated phases was calculated by a conservation equation as described in

our previous work.[44] For example, in the phase-separated PS/PVME/R974 15/85/0.5 blend the volume fraction of the PS-rich phase is obtained as 28%, consequently the volume fraction of the nanoparticles in the PS-rich phase is 1.78%. As shown in Figure 9, the addition of R974 nanosilica increases the dynamic asymmetry which intensifies as the volume fraction of nanoparticles is increased. However, R974 nanoparticles affect mostly the dynamic asymmetry of the blends with lower PS content. As discussed above, upon incorporation of 1% R974 to the 30/70 blend, the mechanism changes from SD into VPS. According to Figure 9, such concentration of nanosilica increases the amount of dynamic asymmetry to about 56%. 117% increase of dynamic asymmetry in 40/60 blend through addition of 2% nanosilica, changes NG to VPS.

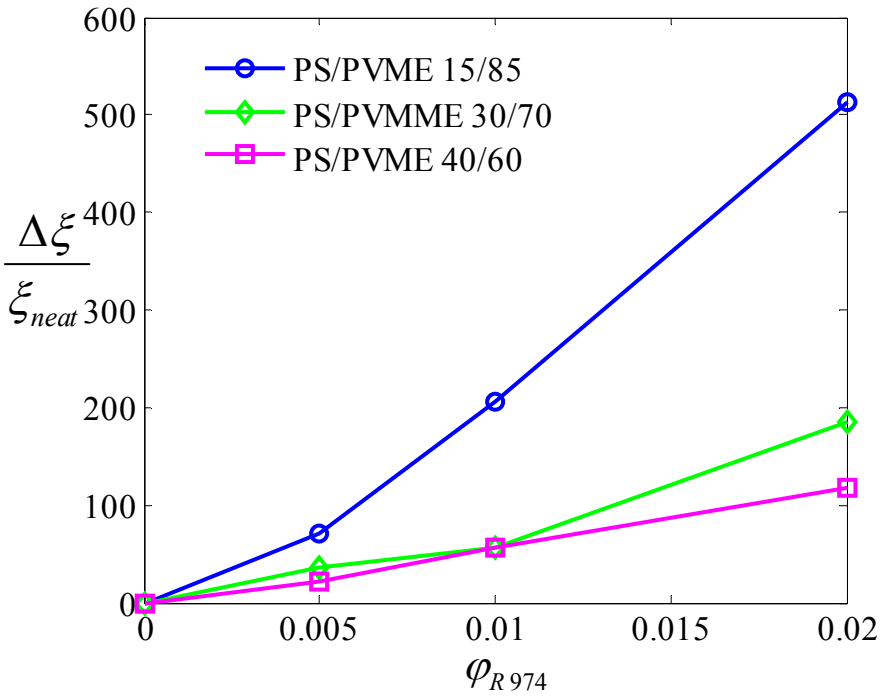

Figure 9. Relative change of dynamic asymmetry as a function of volume fraction of R974 nanosilica for PS/PVME blends.

3.2.3. PS/PVME/A200 blends

Due to the preferential attraction of A200 nanoparticles to PVME polymer, it is expected that dynamic asymmetry in the PS/PVME blend decreases by addition of A200 nanoparticles.

Viscoelastic phase separation region, PS/PVME 15/85 blend.

Figure 9a shows the morphological development of the PS/PVME 15/85 blend in the presence of 0.5% A200 nanosilica at 110 ^{o}C. The phase separation of this blend undergoes TG-VPS mechanism similar to the neat one. However, the characteristic domains size becomes smaller with respect to the neat blend in similar phase separation times indicative of slower phase separation kinetics. The addition of A200 nanoparticles induces a faster phase inversion due to a decrease in dynamic asymmetry between the PS-rich and PVME-rich phases. During the VPS, self-generated stresses inhibit the interfacial forces from disconnecting the network structure until the stresses relax in the late stage of phase separation. This coincides with the concentration of phase separated-domains reaching the final equilibrium value. With suppressing dynamic asymmetry, the stress fields will be weaker, the relaxation of self-generated stresses becomes faster, and thus, the phase inversion occurs earlier. Our findings are consistent with the simulation results, which show the phase inversion takes place earlier with decreasing the extent of dynamic asymmetry.[15] Similar behavior is observed in presence of 1% A200 nanosilica (not shown here).

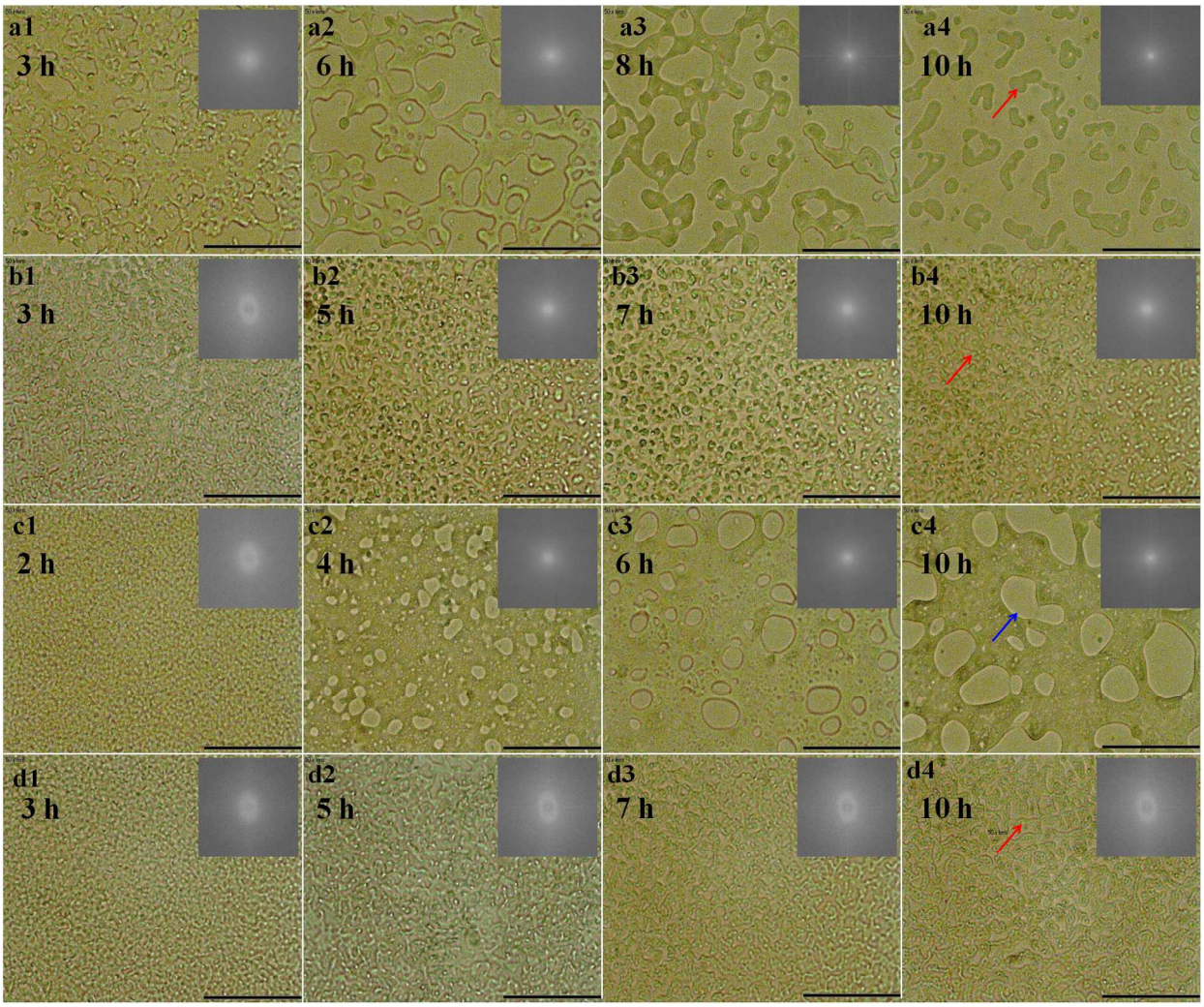

Figure 10. Optical micrographs indicating time evolution of the phase-separating morphologies at 110 ^{o}C for PS/PVME/A200 blends: (a) 15/85/0.5, (b) 15/85/2, (c) 30/70/0.5, and (d) 30/70/2. All the scale bars correspond to 30 μm . Optical micrographs indicating time evolution of the phase-separating morphologies at 110 ^{o}C for PS/PVME 30/70 blend containing R974 nanosilica with volume fraction of: (a) 0%, (b) 1%, and (c) 2%. All the scale bars correspond to 30 μm . The insets show correspondding two-dimensional fast Fourier transform pattern, 2D-FFT. The red and blue arrows indicate PS-rich and PVME-rich phases, respectively.

By further increasing the amount of A200 nanosilica to 2%, VPS disappears and phase separation takes place through SD mechanism (Figure 9b). In the early stage of phase separation, an interconnected structure is developed as a characteristic of SD, which breaks up into dispersed PS-rich domains in the PVME-rich matrix at longer times. The emergence of ring in the corresponding 2D-FFT patterns also shows that phase separation proceeds via SD mechanism. The mechanism transition can be attributed to the reduced dynamic asymmetry in the presence of hydrophilic nanoparticles.

DSC and rheological measurements can be used to study the decreased dynamic asymmetry upon introducing A200 nanoparticles. As the wetting parameter suggests (Equation 7) and will be shown by TEM images, the hydrophilic nanoparticles will be localized selectively in the PVME-rich phase during the phase separation. According to the phase diagram, the composition of PVME-rich phase at 110 ^{o}C is about PS/PVME 2/98, which was prepared as described in the Experimental Section. Figure 10a shows the effect of A200 nanoparticles on glass-transition temperature of the PVME-rich phase. T_g of the PVME-rich phase increases considerably with the addition of hydrophilic nanosilica. Therefore, there is an attractive interaction between polymer molecules and nanoparticles, which restricts the chain mobility in the PVME-rich phase and decreases the difference between the molecular mobility in the PS-rich and PVME-rich phases. As a result, dynamic asymmetry is reduced. The interaction between the A200 nanoparticles and PVME-rich molecules occurs through the hydrogen bonding between the ether oxygen of PVME molecules and isolated silanol groups on the silica surface.

The values of ΔC_p at glass transition temperature for the PVME-rich phase filled with different concentrations of nanosilica are shown in Figure 10b. ΔC_p decreases monotonically with nanosilica content indicating a restricted mobility of the polymer chains.[64]

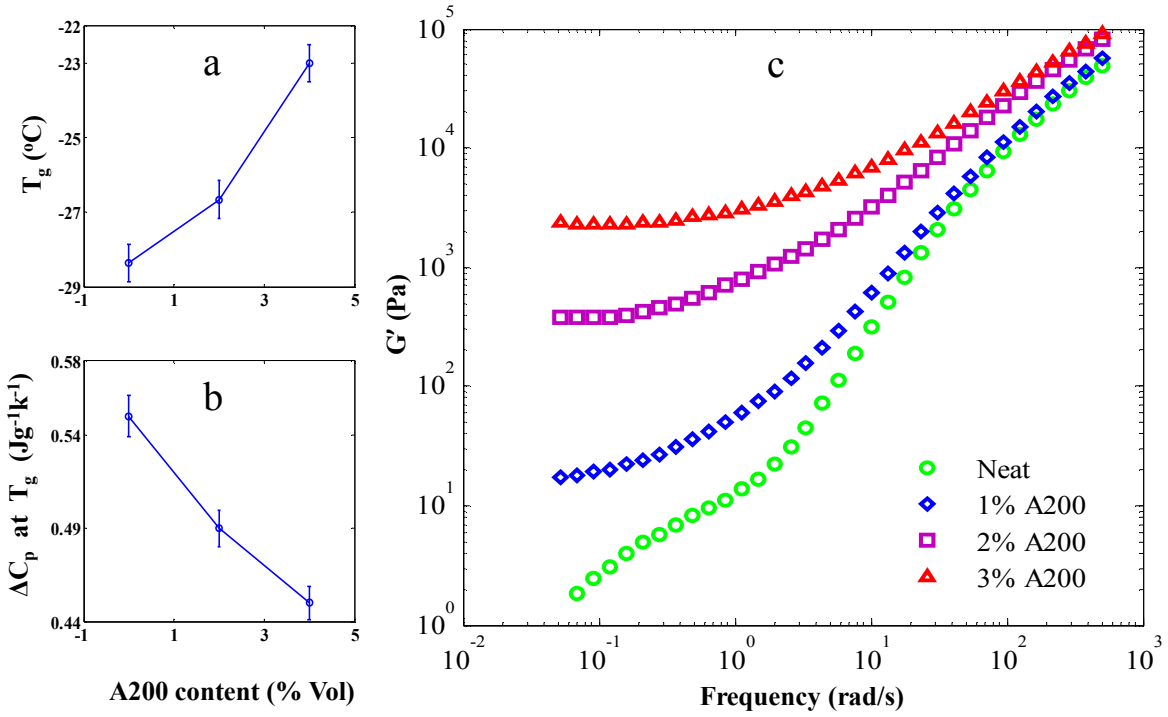

Figure 11. a) Values of T_g for PVME-rich phase as a function of nanosilica content; b) change in heat capacity (ΔC_p) of the PVME-rich phase at glass transition as a function of nanosilica content. and c) frequency-dependent storage modulus of PVME-rich phase containing different volume fractions of A200 nanosilica at 110 °C. Vertical lines in parts a and b represent error bars.

Figure 10c shows the effect of A200 nanoparticles on elasticity of the PVME-rich phase at 110 °C. Hydrophilic nanoparticles affect the PVME-rich elasticity dramatically even at volume fractions as low as 1%. As the particle loading increases, the dependence of G' on ω weakens and storage modulus increases especially at low frequencies. At particle volume fraction of 2%, G' becomes almost independent of ω at low frequencies demonstrating that nanoparticles restrains the long-range motion of polymer chains. The G' ratio of pure PS-rich phase to PVME-rich at frequency of 0.1 at 110 °C decreases from ~1990 to ~26 with addition of 2% A200 to

PVME-rich phase (Figure 7c and 10c), which means dynamic asymmetry is suppressed considerably.

Spinodal decomposition region, PS/PVME 30/70 blend.

Figure 9c shows the morphology development of PS/PVME 30/70 blend in the presence of 0.5% A200 nanosilica at 110 ^{o}C. For this blend phase separation undergoes SD mechanism similar to the neat one. The interconnected co-continuous structure develops in the early stage of phase separation and breaks up into PVME-rich droplets in PS-rich matrix in the late stage. The co-continuous structure has a longer life in the presence of nanoparticles. However, after the structural breakup, PVME-rich droplets size in PS/PVME/A200 blend is much smaller than in the neat blend at similar phase separation times, which suggests the capability of A200 nanoparticles to slow down the kinetics of phase separation even at volume fractions as low as 0.5%. Similar behavior is observed in the presence of 1% A200 nanosilica (not shown here). Figure 11a shows the TEM micrograph of PS/PVME/A200 30/70/0.5 blend annealed at 110 ^{o}C for 7 hr. As seen, the nanoparticles are entirely located in the PVME-rich phase. This is consistent with the prediction of wetting parameter (Equation 7).

With further increasing the concentration of hydrophilic nanoparticles to 2% in the 30/70 blend, phase separation proceeds through SD as expected and an interconnected structure is developed in the early stage of phase separation (Figure 9d). However, the co-continuous morphology becomes very stable and remains unchanged after 5 hr, demonstrating the pinning of the structure by nanoparticles. Figure 11b shows TEM image of PS/PVME/A200 30/70/2 blend after 7 hr annealing at 110 ^{o}C. Nanoparticles are percolated in the PVME-rich phase similarly to the arrested morphology in PS/PVME/R974 15/85/2 blend. It should be noted that while the double percolation occurs through the PS-rich phase in the PS/PVME blends containing 2% R974, it

takes place through the formation of hydrophilic silica network in the PVME-rich phase. As mentioned in the Introduction section, stabilizing the co-continuous structure is a scientific and industrial challenge. The key point of the current study is that instead of using nanoparticles with carefully controlled surface chemistry to achieve neutral wetting or dual nature like Janus particles, nanoparticles with preferential wettability can be used to provide a more economic approach to arrest co-continuous morphologies. Addition of A200 nanoparticles to PS/PVME 40/60 blend only slows down the kinetics of phase separation without changing the phase separation behavior (not shown here).

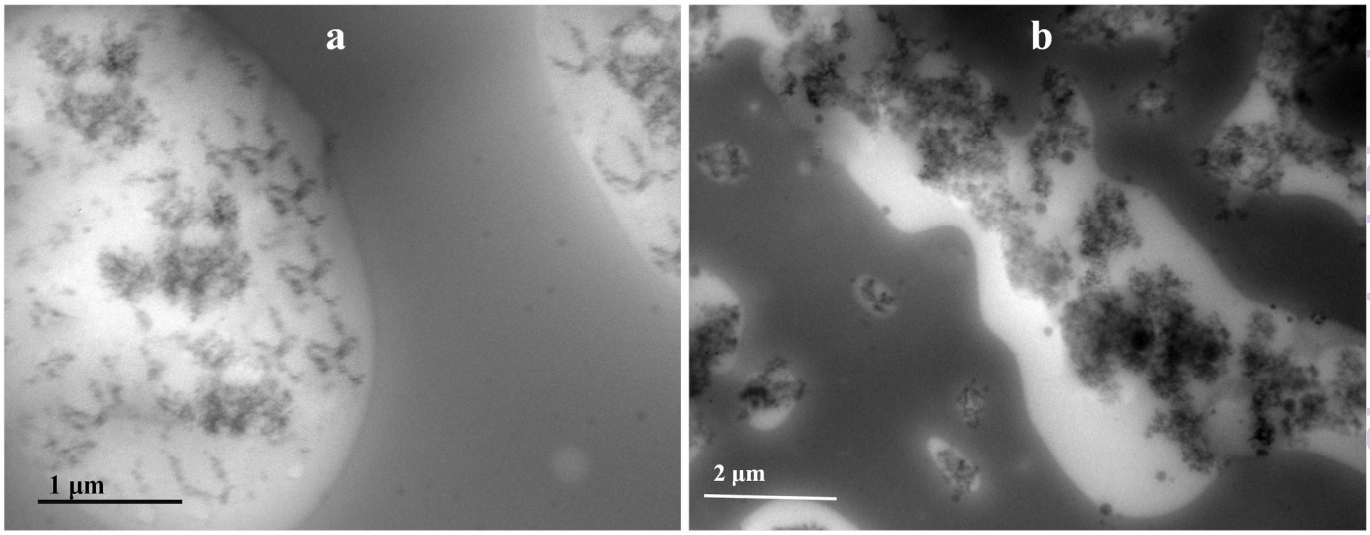

Figure 12. TEM images of PS/PVME/A200 blends annealed at 110 ^{o}C for 7 hr: a) 30/70/0.5 blend, b) 30/70/2 blend.

Figure 13 shows the relative change of the dynamic asymmetry versus volume fraction of A200 nanosilica for all PS/PVME blends studied. The addition of A200 nanosilica decreases the dynamic asymmetry that intensifies as the volume fraction of nanoparticles is increased. As discussed above, upon incorporation of 2% A200 nanosilica to the 15/85 blend, the mechanism

changes from VPS to SD. According to Figure 13, such concentration of nanosilica decreases the amount of dynamic asymmetry about 74%. For the 40/60 blend, the addition of 2% nanosilica which corresponds to 100% increase of dynamic asymmetry, changes NG to VPS.

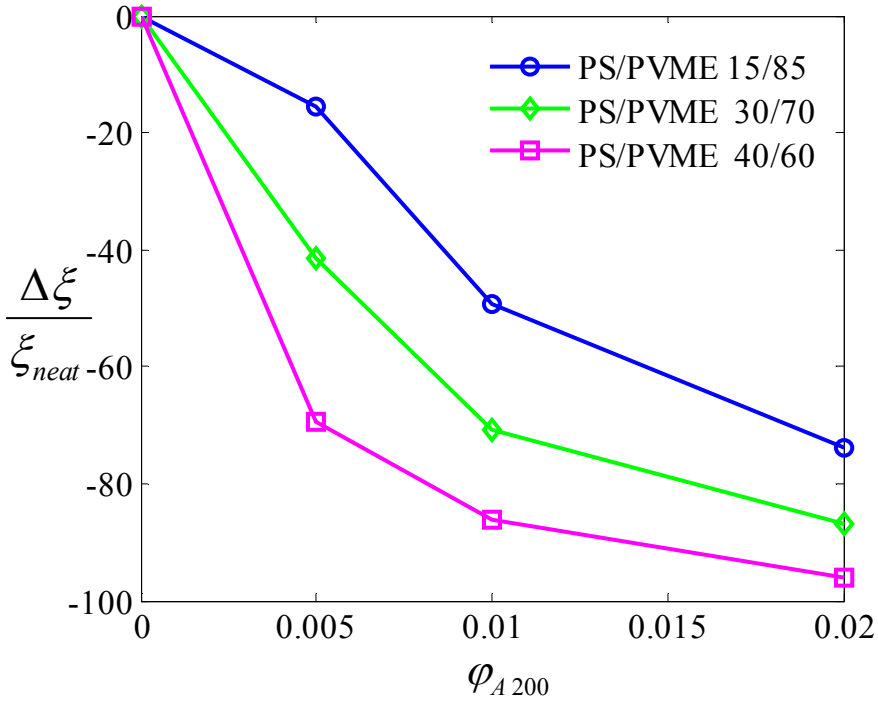

Figure 13. Relative change of dynamic asymmetry as a function of volume fraction of A200 nanosilica for PS/PVME blends.

We can estimate the diffusion coefficient of the nanoparticles with radius r using Stokes-Einstein relation:[28,69]

$$D = \frac{k_B T}{6\pi\eta r} \qquad (11)$$

In this equation, k_B is the Boltzmann constant, and η is the viscosity of media at temperature T. The viscosity of the blend is about 10^4 Pa.s for PS/PVME 30/70 blend at 110 ^oC, which yields the diffusion coefficient of nanoparticles and their aggregates in the range of

$5.61-46.7\times10^{-15}\ cm^2/s$. The time required for the nanoparticles to diffuse over their diameter can be calculated as $t_r = r^2/D$. Therefore, nanoparticles and their aggregates need ~7.7–557 sec to diffuse a distance equal to their size.

3.3. Kinetics of phase separation

Coarsening of the phase-separating domains with time can be characterized by a power law dependence, $d \propto t^m$, where m is an exponent, depending on the coarsening mechanism.[44] For droplet-matrix phase separation, Ostwald ripening (Lifshitz-Slyozov theory) and Brownian-coagulation (Binder-Stauffer theory) mechanisms are dominant.[66,67] The driving force for these two mechanisms is the diffusion of molecules or droplets. The coarsening of the domains with time for both mechanisms is described by m=1/3. For SD mechanism, the coarsening of domains is due to the hydrodynamic flow driven by capillary forces and is described by m=1 (Siggia's theory).[70] There is no theory for predicting domain size growth of network structure for samples with VPS mechanism.

Figure 14 shows the variation of domain size (PVME-rich phase) with time for neat and filled PS/PVME blends. The characteristic length scale for the samples with co-continuous morphology induced by SD mechanisms is obtained by the $d = 2\pi/q_m$ equation,[71,72] where q_m is the scattering vector associated with the maximum scattering intensity value in the radially averaged 2D-FFT spectrum (not shown here), which can be obtained[71] from the insets shown in optical micrographs. However, for samples phase-separating by NG or VPS, ring formation cannot be observed in 2D-FFT pattern; consequently, scattered light intensities increase with time without displaying a scattering maximum. Therefore, for samples undergoing NG or VPS, we obtained the average domain size directly by image analysis of optical micrographs.

Figure 14a,d shows that the exponent m is nearly 1.6 for the neat PS/PVME 15/85 blend which is fairly close to the $d \propto t^{3/2}$ scaling obtained by Tanaka[13] for samples with VPS mechanism. It can be seen that addition of either A200 or R974 nanosilica decreases the average domain size and the exponent m, indicating the slowdown of phase separation. However, the decrease of m in the presence of nanoparticles is more pronounced and in the sample containing 2% nanosilica, a single power-law model cannot fit the experimental data points. Reaching to a plateau in domain growth at long times for samples containing 2% nanosilica indicates the pinning of phase separation and high efficiency of the nanoparticles in suppressing phase separation. Figure 14b,e shows that the exponent m is nearly 1 for neat 30/70 PS/PVME blend indicating that the coarsening of the domains in spinodal region is mainly driven by hydrodynamic flow mechanism that is in agreement with the prediction of Siggia's theory. Figure 14c,f shows that the exponent m is about 0.5 (more than 1/3 predicted by Lifshitz-Slyozov or Binder-Stauffer theories for droplet coarsening) for neat 40/60 blend, as was observed by Vinckier[73] and Bousmina[74] et al. for NG phase separating system. This result indicates a second process (in addition to the diffusion process) involved in the structure evolution. The Ostwald ripening and Brownian coagulation mechanisms ignore the interaction between droplets. Therefore, both mechanisms are valid only in the limit of low volume fractions. When the volume fraction of dispersed phase becomes higher, hydrodynamic flow fields start playing an important role that could increase the rate of droplet size change.

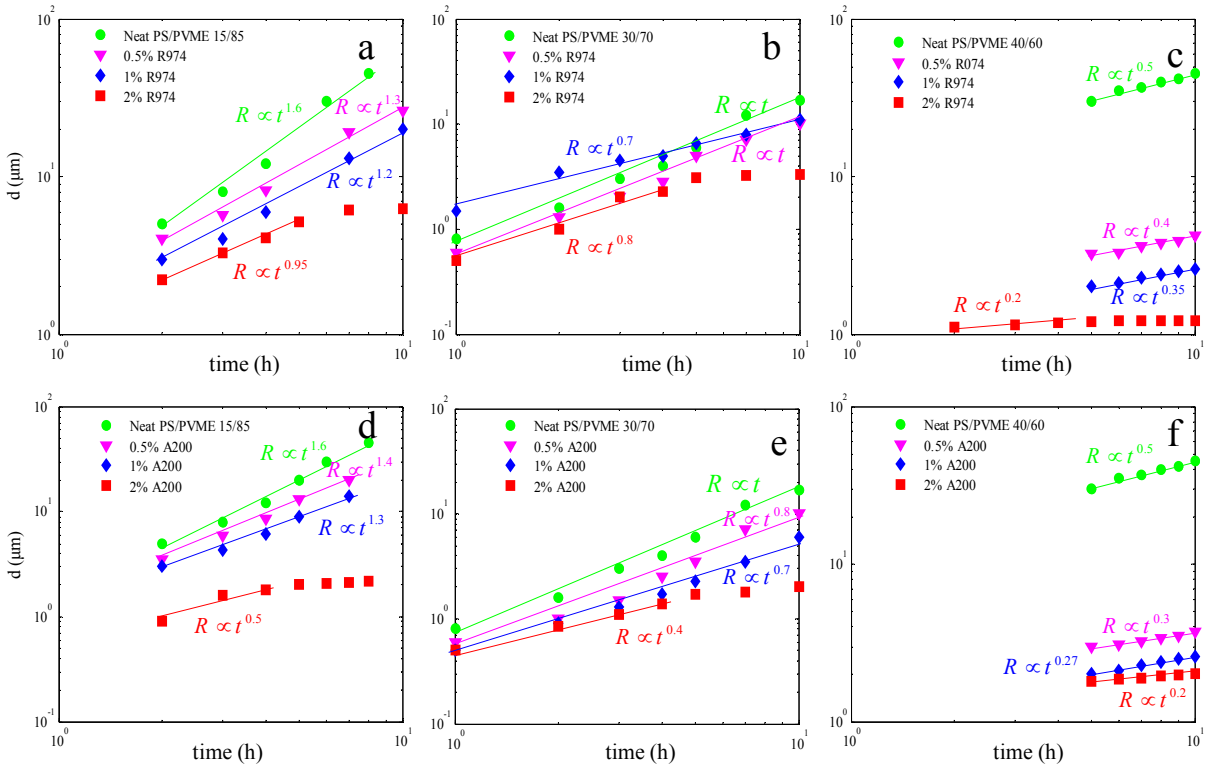

Figure 14. The variation of domain size (PVME-rich phase) with time for phase-separating PS/PVME blends with different concentrations of R974 and A200 nanosilica at 110 °C.

To further elucidate the kinetics of phase separation, as a typical kinetics study, we performed isothermal time sweep experiments of the storage modulus during the phase separation at 110 °C for the PS/PVME 30/70 filled with R974 and A200 nanoparticles. The values of storage modulus are normalized by the initial values, G_o', to have a proper comparison among samples as shown in Figure 12. Time evolution behavior of storage modulus can provide valuable information on the evolution of the morphological changes.[44,75]

For all blend samples, G' initially increases and after passing through a maximum subsequently decreases, consistent with the prediction of time-dependent Ginzburg-Landau (TDGL) theory.[75] The initial increase is due to the combined effect of enhanced concentration fluctuations and

induced interfacial area in the early stages of phase separation. At later stages where domains coarsen and the interfacial area per unit volume decreases, G' decreases. The time corresponding to maximum of G' increases with increasing nanosilica content, which demonstrates a longer duration of the early stage and a slower phase-separating process for higher nanoparticle fraction.

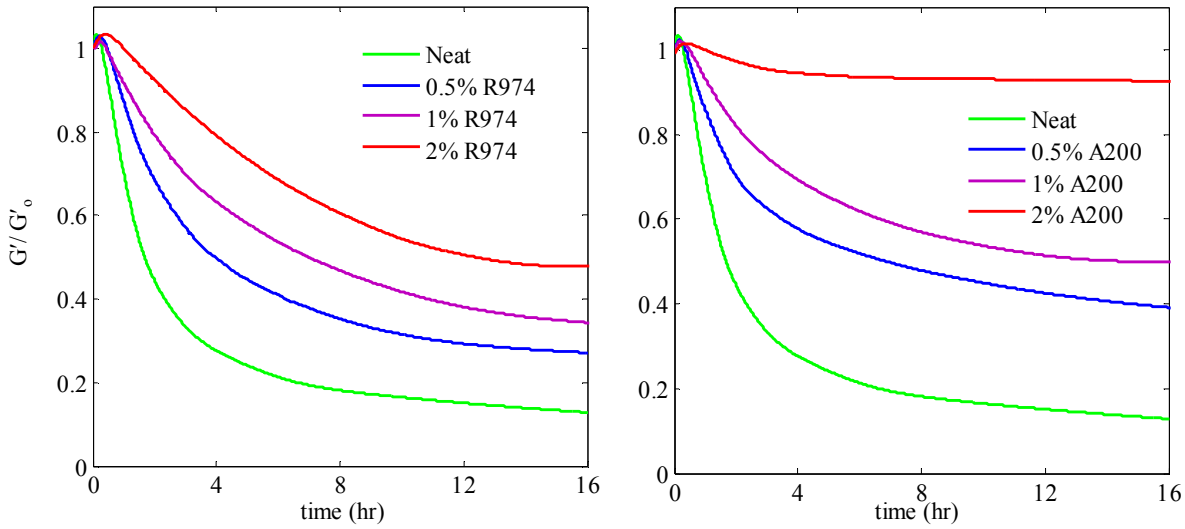

Figure 15. Time evolution of the normalized storage modulus at frequency of 1 rad/s, strain of 1%, and temperature of 110 ^{o}C for PS/PVME 30/70 blend containing different amounts of R974 and A200 nanoparticles.

The rate of evolution of G' indirectly correlates with the kinetics of phase separation. Both types of nanoparticles dramatically slow down the time evolution of G'. For example, even at 0.5% nanoparticles the phase separation kinetics noticeably decreases in agreement with optical microscopy images. This effect is more pronounced in the samples containing hydrophilic nanoparticles as seen in Figure 12. The strong hydrogen bonding between isolated silanol groups on the surface of A200 nanosilica and the ether oxygen of PVME results in a strong restriction on the molecular mobility of PVME, while the affinity of hydrophobic R974 nanoparticles with PS occurs through much weaker van der Waals interactions.

According to the obtained phase diagrams, the thermodynamic phase boundaries do not change considerably by the addition of nanoparticle. Therefore, the observed morphological consequences originate from a change in the kinetics of system (or a pinning phenomenon) rather than changes in its thermodynamic.

It should be noted that there is a competition between formation of nanosilica network and coarsening of phase separated domains in samples, which affects the evolution of G'.[24] Nanoparticles dispersed in polymeric melts tend to aggregate and form network upon annealing, which leads to an enhancement in elasticity. On the other hand, coarsening of phase-separated domains decreases G'. The overall trend of G' depends on the volume fraction of the nanosilica and composition of polymers in the blends. At low volume fractions of nanosilica, coarsening dominates the G' evolution. However, with increase of nanoparticles loading beyond a critical volume fraction, the formation of nanosilica network dominates the G' evolution, which induces continuous increase of G'.[24] In addition, according to the literature for blends closer to the critical composition the coarsening of phases is stronger, and even at high volume fractions of nanosilica G' can decrease with phase separation.[23] Therefore, the trend of G' evolution is a complex combination of volume fraction of nanosilica, polymers, as well as other parameters such temperature. Our results show that the coarsening of phase-separated domain dominates the evolution of G'.

4. Conclusion

In this work, we investigated the use of nanoparticles to control the kinetics and morphology of phase separation in dynamically asymmetric PS/PVME blends. More specifically we utilized two different types of Aerosil silica, hydrophobic R974 and hydrophilic A200 nanoparticles, which

self-assemble during phase separation into the bulk of the slow dynamic phase (PS-rich phase) and fast dynamic phase (PVME-rich phase), respectively. Nanoparticles with preferential wettability can modify the dynamic asymmetry by self-assembling into the preferred phase, and thus, can effectively control the kinetics by slowing down or arresting phase separation if adequate concentration is used. Therefore, more complicated routes for such purposes such using nanoparticles with carefully controlled surface chemistry to achieve neutral wetting or dual nature like Janus particles might not be necessary. Here, both types of nanoparticles significantly slow down the different mechanisms (NG, SD, and VPS) of phase separation at a low volume fraction of 0.5%. The effect intensified as the volume fraction was increased. The VPS and SD phase separations were arrested in the presence of 2 vol% hydrophobic and hydrophilic nanoparticles, due to double percolated structures created in the PS-rich phase and PVME-rich phase, respectively, as confirmed by TEM micrographs. Hydrophobic nanoparticles make the dynamic of the PS-rich phase even slower and promote VPS behavior by enhancing dynamic asymmetry. At 2 vol% of hydrophobic nanoparticles, thermodynamically controlled mechanisms (NG and SD) change to the VPS one. In contrast, hydrophilic nanoparticles slow down the dynamic of the PVME-rich phase and demote VPS behavior by decreasing dynamic asymmetry.

Acknowledgements

We thank Mrs. Tahereh Samaee Yekta (Amirkabir University of Technology) for her assistance in carrying out the morphological observations by optical microscopy. The authors thank Mr. Dimitris Theodorides (University of Crete) for his expert assistance with the TEM imaging.

References

(1) Iwashita, Y.; Tanaka, H. *Nat. Mater.* **2006**, 5, 147-152.

(2) Tanaka, H. *Adv. Mater.* **2009**, 21, 1872-1880.

(3) Yeganeh, J. K.; Goharpey, F.; Foudazi, R. *RSC Adv.* **2014**, 4, 12809–12825.

(4) Lin,Y.; Shangguan,Y.; Chen, F.; Zuo, M.; Zheng, Q. *Polym. Int.* **2013**, 62, 676–683.

(5) Zhang, J.; Ravati, S.; Virgilio, N.; Favis, B. D. *Macromolecules* **2007**, 40, 8817-8820.

(6) Hoppe, H.; Sariciftci, N. S. *J. Mater. Chem.* **2006**, 16, 45–61.

(7) Asadi, K.; Wondergem, H. J.; Moghaddam, R. S.; McNeill, C. R.; Stingelin, N.; Noheda, B.; Blom, P. W. M.; de Leeuw, D. M. *Adv. Funct. Mater.* **2011**, 21, 1887-1894.

(8) Xie, H. Q.; Xu, J.; Zhou, S. *Polymer* **1991**, 32, 95-102.

(9) Liu, Z. H.; Marechal, P.; Jerome, R. *Polymer* **1998**, 39, 1779-1785.

(10) Kesting, R. E. *Synthetic polymeric membranes: a structural perspective*, Wiley-Interscience: New York, **1985**, p 368.

(11) Sperling, L. H. *Introduction to Physical Polymer Science*, John Wiley & Sons, Hoboken, New Jersey **2006**.

(12) Tanaka, H. *Phys. Rev. Lett.* **1993**, 71, 3158-3161.

(13) Tanaka, H. *Phys. Rev. Lett.* **1996**, 76, 787-790.

(14) Shi,W.; Yang, J.; Liu,W.; Zhang, L.; Han, C. C. *Macromolecules* **2013**, 46, 2516−2520

(15) Zhang, J.; Zhang, Z.; Zhang, H.; Yang, Y. *Phys. Rev. E* **2001**, 64, 051510.

(16) Koyama, T.; Tanaka, H. *Europhys. Lett.* **2007**, 80, 68002.

(17) Herzig, E. M.; White, K. A.; Schofield, A. B.; Poon,W. C. K.; Clegg, P. S.; *Nat. Mater.* **2007**, 6, 966-971.

(18) Lee, M. N.; Mohraz, A. *Adv. Mater.* **2010**, 22, 4836–4841.

(19) Jiang, S.; Chen, Q.; Tripathy, M.; Luijten, E.; Schweizer, K. S.; Granick, S. *Adv. Mater.* **2010**, 22, 1060–1071.

(20) Walther, A.; Muller, A. H. E. *Chem. Rev.* **2013**, 113, 5194-5261.

(21) Bharati, A.; Xavier, P.; Kar, G. P.; Madras, G.; Bose, S. *J. Phys. Chem. B* **2014**, 118, 2214−2225.

(22) Gao, J.; Huang, C.; Wang, N.; Yu, W.; Zhou, C. *Polymer* **2012**, 53, 1772-1782.

(23) Gharachorlou, A.; Goharpey, F. *Macromolecules* **2008**, 41, 3276-3283.

(24) Xia, T.; Huang, Y.;Jiang, X.; Lv, Y.;Yang, Qi,; Li, G. *Macromolecules* **2013**, 46, 8323-8333.

(25) Li, L.; Miesch, C.; Sudeep, P. K.; Balazs, A. C.; Emrick, T.; Russell, T. P.; Hayward, R. C. *Nano Lett.* **2011**, 11, 1997–2003.

(26) Yziquel, F.; Carreau, P.J.; Tanguy, P.A. *Rheol. Acta* **1999**, 38, 14-25.

(27) Huang, Y.; Jiang, S.; Li, G.; Chen, D. *Acta Mater.* **2005**, 53, 5117−5124.

(28) Huang, C.; Gao, J.; Yu, W.; Zhou, C. *Macromolecules* **2012**, 45, 8420−8429.

(29) Yeganeh, J. K.; Goharpey, F.; Moghimi, E.; Petekidis, G.; Foudazi, R. *Soft Matter* **2014**, 10, 9270-9280.

(30) Laradji, M.; MacNevin, G. *J. Chem. Phys.* **2003**, 119, 2275–2284.

(31) Zhu, Y. J.; Ma, Y. Q. *Phys. ReV. E* **2003**, 67, 041503.

(32) Ginzburg, V. V.; Qiu, F.; Paniconi, M.; Peng, G.; Jasnow, D.; Balazs, A. C. *Phys. ReV. Lett.* **1999**, 82, 4026–4029.

(33) Balazs, A. C.; Ginzburg, V. V.; Qiu, F.; Peng, G.; Jasnow, D. *J. Phys.Chem. Part B* **2000**, 104, 3411–3422.

(34) Ginzburg, V. V.; Peng, G.; Qiu, F.; Jasnow, D.; Balazs, A. C. *Phys.ReV. E* **1999**, 60, 4352–4359.

(35) Yeganeh, J. K.; Goharpey, F.; Foudazi, R. *RSC Adv.* **2012**, 2, 8116-8127.

(36) Kapnistos, M.; Hinrichs, A.; Vlassopoulos, D.; Anastasiadis, S. H.; Stammer, A.; Wolf, B. A. *Macromolecules* **1996**, 29, 7155-7163.

(37) V. J. Klenin, *Thermodynamics of systems containing flexible chain polymers*, Elsevier, Amsterdam, **1999**, p. 312.

(38) Kim, J. H.; Kwei, T. K.; Pearce, E. M. *Chem. Eng. Comm.* **1992**, 116, 105-116.

(39) Reich, S.; Cohen, Y. *J. Polym. Sci., Polym. Phys. Ed.* **1981**, 19, 1255-1267.

(40) Sharma, J.; Clarke, N. *J. Phys. Chem. B* 2004, **108**, 13220-13230.

(41) Kim, J. K.; Son, H. W.; Lee, Y.; Kim, J. *J. Polym. Sci., Part B:Polym. Phys.* **1999**, 37, 889-906.

(42) Polios, I. S.; Soliman, M.; Lee, C.; Gido, S. P.; Roher, K. S.; Winter, H. H. *Macromolecules* **1997**, 30, 4470-4480.

(43) Zou, F.; Dong, X.; Liu, W.; Yang, J.; Lin, D.; Liang, A.; Li, W.; Han, C. C. *macromolecules* **2012**, 45, 1692-1700.

(44) Yeganeh, J. K.; Goharpey, F.; Foudazi, R. *Macromolecules* **2010**, 43, 8670-8685.

(45) Ajji, A.; Choplin, L. *Macromolecules* **1991**, 24, 5221-5223.

(46) Fredrickson, G. H.; Larson, R. G. *J. Chem. Phys.* **1987**, 86, 1553–1560.

(47) Xavier, P.; Bose, S. *J. Phys. Chem. B* **2013**, 117, 8633-8646.

(48) Vandebril, S.; Vermant, J.; Moldenaers, P.; *Soft Matter* **2010**, 6, 3353–3362.

(49) Owens, D. K.; Wendt, R. C. *J. Appl. Polym. Sci.* **1969**, 13, 1741-1747.

(50) Elias, L.; Fenouillot, F.; Majeste, J.C.; Cassagnau, P. *Polymer* **2007**, 48, 6029-6040.

(51) Liu, K.; Kiran, E. *J. Supercrit. Fluids*, 1999, 16, 59–79.

52- Xiong, Y.; Kiran, E. *Rev. Sci. Instrum.*, 1998, 69,1463- 1471.

(53) Yan, L. T.; Xie, X. M. *Prog.Polym.Sci.* **2013**, 38, 369–405.

(54) Brown, D.; Mele, P.; Marceau, S.; Alberola, N. D. *Macromolecules* **2003**, 36, 1395–1406.

(55) Tanaka, H.; Araki, T. *Europhys. Lett.* **2007**, 79, 58003.

(56) Koyama, T.; Araki, T.; Tanaka, H. *Phys. Rev. Lett.* **2009**, 102, 065701.

(57) Guo, Z.; Pereira, T.; Choi, O.; Wang, Y.; Hahn, H. T. *J. Mater. Chem.* **2006**, 16, 2800–2808

(58) Wu, C. L.; Zhang, M. Q.; Rong, M. Z.; Friedrich, K. *Comp. Sci.Technol.* **2002**, 62, 1327–1340

(59) Gao, X.; Zhang, S.; Mai, F.; Lin, L.; Deng, Y.; Deng, H.; Fu, Q. *J. Mater. Chem.* **2011**, 21, 6401–6408.

(60) Li, Y.; Shimizu, H. *Macromolecules* **2008**, 41, 5339-5344

(61) Meincke, O.; Kaempfer, D.; Weickmann, H.; Friedrich, C.; Vathauer, M.; Warth, H. *Polymer* **2004**, 45,739–748.

(62) Filippone, G.; Romeo, G.; Acierno, D. *Langmuir* **2010**, 26, 2714–2720.

(63) Araki, T.; Tanaka, H. *Macromolecules* **2001**, 34, 1953-1963.

(64) Zhang, X.; Loo, L. S. *Macromolecules* **2009**, 42, 5196–5207.

(65) Du, F.; Scogna, R.C.; Zhou, W.; Brand, S.; Fischer, J. E.; Winey, K.I. *Macromolecules* **2004**, 37, 9048-9055.

(66) Lifshitz, I. M.; Slyozov, V. V. *J. Phys. Chem. Solids* **1961**, 19, 35–50.

(67) Binder, K.; Stauffer, D. *Phys. Rev. Lett.* **1974**, 33, 1006–1009.

(68) Xia, T.; Huang, Y.; Peng, X.; Li, G. *Macromol. Chem. Phys.* **2010**, 211, 2240–2247.

(69) Foudazi, R.; Nazockdast, H. *J. Appl. Polym. Sci.* **2013**, 3501- 3511.

(70) Siggia, E. D. *Phys. Rev. A* **1979**, 20, 595–605.

(71) Loren, N.; Langton, M.; Hermansson, A. M. *J. Chem. Phys.* **2002**, 116, 10536-10546.

(72) Niu, Y.; Yang, L.; Shimizu, K.; Pathak, J. A.; Wang, H.; Wang, Z. *J. Phys. Chem. B* **2009**, 113, 8820–8827.

(73) Vinckier, I.; Laun, H. M. *Rheol. Acta* **1999**, 38, 274–286.

(74) Mabrouk, K. E.; Bousmina, M. *Rheol. Acta* **2006**, 45, 877–889.

(75) Zhang, Z. L.; Zhang, H. D.; Yang, Y. L.; Vinckier, I.; Laun, H. M. *Macromolecules* **2001**, 34, 1416-1429.

Graphical Abstract

Manipulating the Kinetics and Mechanism of Phase Separation in Dynamically Asymmetric LCST Blends by Nanoparticles